

Fourier-Domain Beamforming: The Path to Compressed Ultrasound Imaging

Tanya Chernyakova, *Student Member, IEEE*, and Yonina C. Eldar, *Fellow, IEEE*

Abstract—Sonography techniques use multiple transducer elements for tissue visualization. Signals received at each element are sampled before digital beamforming. The sampling rates required to perform high-resolution digital beamforming are significantly higher than the Nyquist rate of the signal and result in considerable amount of data that must be stored and processed. A recently developed technique, compressed beamforming, based on the finite rate of innovation model, compressed sensing (CS), and Xampling ideas, allows a reduction in the number of samples needed to reconstruct an image comprised of strong reflectors. A drawback of this method is its inability to treat speckle, which is of significant importance in medical imaging. Here, we build on previous work and extend it to a general concept of beamforming in frequency. This allows exploitation of the low bandwidth of the ultrasound signal and bypassing of the oversampling dictated by digital implementation of beamforming in time. By using beamforming in frequency, the same image quality is obtained from far fewer samples. We next present a CS technique that allows for further rate reduction, using only a portion of the beamformed signal's bandwidth. We demonstrate our methods on *in vivo* cardiac data and show that reductions up to 1/28 of the standard beamforming rates are possible. Finally, we present an implementation on an ultrasound machine using sub-Nyquist sampling and processing. Our results prove that the concept of sub-Nyquist processing is feasible for medical ultrasound, leading to the potential of considerable reduction in future ultrasound machines' size, power consumption, and cost.

I. INTRODUCTION

DIAGNOSTIC ultrasound has been used for decades to visualize body structures. Imaging is performed by transmitting a pulse along a narrow beam from an array of transducer elements. During its propagation, echoes are scattered by acoustic impedance perturbations in the tissue and received by the array elements. The data collected by the transducers is sampled and digitally integrated in a way referred to as beamforming. The process of beamforming comprises averaging the received signals after their alignment with appropriate time-dependent delays. Beamforming allows one to obtain a signal steered in a predefined direction, corresponding to the transmission path, and optimally focused at each depth. This results in SNR enhancement and improvement of angular localization. Such a beamformed signal, referred to as a beam, forms a line in the image.

According to the classic Shannon–Nyquist theorem [1], the minimal sampling rate at each transducer element should be at least twice the bandwidth of the received signal to avoid aliasing. In practice, rates up to 4 to 10 times the central frequency of the transmitted pulse are required to eliminate artifacts caused by digital implementation of beamforming in time [2]. Taking into account the number of transducer elements and the number of lines in an image, the amount of sampled data that must be digitally processed is very large, motivating methods to reduce sampling and processing rates. The reduction in rate and, consequently, in amount of data can be particularly beneficial for portable devices and wireless probes.

A. Related Work

A possible approach to sampling rate reduction is introduced in [3]. Tur *et al.* consider the ultrasound signal received at each array element within the framework of finite rate of innovation (FRI) [4]. The received signal is modeled as L replicas of a known transmitted pulse, caused by its scattering from reflectors, located along the transmitted beam. Such an FRI signal is fully described by $2L$ parameters, corresponding to the replica's unknown delays and amplitudes. These parameters are recovered from a subset of at least $2L$ of the signal's Fourier series coefficients using array processing methods or compressed sensing (CS) techniques [5], [6]. The required Fourier coefficients can be computed from appropriate low-rate samples of the signal following ideas of [3] and [7]–[10]. Recent work has developed a hardware prototype implementing the suggested sub-Nyquist system in the context of radar [11].

The FRI structure of an ultrasound signal is exploited in a similar fashion in [12] in the context of ultrasonic flaw detection with a single-element transmitter and receiver. The unknown parameters are recovered from sub-Nyquist samples of the received signal, projected on a random Bernoulli basis. To simplify the sampling process [13] proposes a digital-assisted asynchronous CS front-end. In this approach, the received signal is not directly sampled, but rather first converted into ternary timing information, allowing for significant reduction in the system's complexity. A CS approach is also used in [14] to recover the raw received signals by exploiting sparsity in the wave atom domain. Here, low-rate samples of the received signals are obtained by random subsampling of the original data.

The preceding frameworks allow sampling and recovery of each individual received signal at a low rate, assuming sufficiently high SNR. However, the final goal in low-rate

Manuscript received February 4, 2014; accepted April 28, 2014.

The authors are with the Department of Electrical Engineering, Technion, Israel Institute of Technology, Haifa, Israel (e-mail: ctanya@tx.technion.ac.il).

DOI <http://dx.doi.org/10.1109/TUFFC.2014.3032>

ultrasound imaging is to recover a two-dimensional image. Such an image is obtained by integrating the noisy data sampled at multiple transducer elements. In standard imaging, the integration is achieved by the process of beamforming, which is performed digitally and, theoretically, requires high sampling rates. Hence, to benefit from the rate reduction achieved at the level of the received signals, one must be able to incorporate beamforming into the low-rate sampling process. Several works describe methods for recovering a beamformed signal from its low-rate samples using CS methodology [15]–[17]. However, these techniques all assume that one has access to the continuous-time beamformed data. In practice, the beamformed signal is formed from samples of each of the individual received signals. Samples of the beamformed signal are not available at the transducer elements. Therefore, a practical way to acquire low-rate beamformed data from low-rate samples of the received signals is still lacking.

A solution to low-rate beamforming is proposed in [5], where Wagner *et al.* introduce the concept of compressed beamforming. They show that their approach, applied to an array of transducer elements, allows reconstruction of a two-dimensional ultrasound image depicting macroscopic perturbations in the tissue. To develop their method, the authors first prove that the beam obeys an FRI model, implying that it can be reconstructed from a small subset of its Fourier coefficients. However, this required subset cannot be obtained by the schemes proposed in [3] and [7], because the beam does not exist in the analog domain. This fundamental obstacle is resolved by transforming the beamforming operator into the compressed domain. Specifically, Wagner *et al.* show that the Fourier coefficients of the beam can be approximated by a linear combination of Fourier coefficients of the received signals. The latter are obtained from the low-rate samples of the received signals, using the Xampling method, proposed in [3], [7], and [11].

B. Contributions

In this paper, we build on the results in [5] and show that compressed beamforming can be extended to a much more general concept of beamforming in frequency. The core of compressed beamforming is the relationship between the beam and the received signals in the frequency domain, whereas the notion of “compressed” stems from the fact that the Fourier coefficients of the received signals can be obtained from their low-rate samples. Here we show that this frequency-domain relationship is general and holds irrespective of the FRI model. This leads to an approach of beamforming in frequency which is completely equivalent to beamforming in time applicable to any signal, without the need to assume a structured model. When structure exists, beamforming in frequency may be combined with CS to yield further rate reduction.

We note that the concept of beamforming in frequency was first considered back in the 1960s in the context of sonar array processing, operating in the far field [18], [19]. However in contrast to beamforming in the far field, which

is linear in time, the processing required in ultrasound is nonlinear. Its translation to the frequency domain is therefore much more involved and, to the best of our knowledge, was first addressed in [5].

We show that beamforming in frequency allows one to bypass the oversampling dictated by digital implementation of beamforming in time. Because the beam is obtained directly in frequency, we must compute its Fourier coefficients only within its effective bandwidth. We demonstrate that this can be achieved using generalized samples of the received signals, obtained at their effective Nyquist rate. To avoid confusion, by effective Nyquist rate, we mean the signal’s effective band-pass bandwidth, which is typically much lower than its highest frequency. This is because the received signal is normally modulated onto a carrier and only occupies a portion of the entire bandwidth. Using *in vivo* cardiac data, we illustrate that beamforming in frequency allows preservation of image integrity with an 8-fold reduction in the number of samples used for its reconstruction.

Further reduction in sampling rate is obtained, similarly to [5], when only a portion of the beam’s bandwidth is used. In this case, beamforming in frequency is equivalent to compressed beamforming. The received signals are sampled at sub-Nyquist rates, leading to up to 28-fold reduction in sampling rate. Our contribution in this scenario regards the reconstruction method used to recover the beam from its partial frequency data. To estimate the unknown parameters corresponding to the FRI model of the beam, Wagner *et al.* assume that the parameter vector is sparse. The parameters are then obtained by solving an l_0 optimization problem. Sparsity holds when only strong reflectors are taken into account, while the speckle is treated as noise. To capture the speckle, we assume that the parameter vector is compressible and recast the recovery as an l_1 optimization problem. We show that these small changes in the model and the CS reconstruction technique allow one to capture and recover the speckle, leading to significant improvement in image quality.

Finally, we introduce an implementation of beamforming in frequency and sub-Nyquist processing on a stand-alone ultrasound machine and show that our proposed processing is feasible in practice using real hardware. Low-rate processing is performed on the data obtained in real-time by scanning a heart with a 64-element probe. Our approach allows for significant rate reduction with respect to the lowest processing rates that are achievable today, which can potentially impact system size, power consumption, and cost.

The rest of the paper is organized as follows: in Section II, we review beamforming in time and discuss the sampling rates required for its digital implementation. Following the steps in [5], we describe the principles of frequency-domain beamforming in Section III, and prove that it is equivalent to standard time-domain processing. In Section IV, we show that beamforming in frequency allows for rate reduction even without exploiting the FRI model and can be performed at the effective Nyquist rate

TABLE I. LIST OF NOTATION.

| | |
|-----------------------------------|--|
| $\varphi_m(t)$ | Signal received at the m th transducer element |
| $\hat{\varphi}_m(t; \theta)$ | Dynamically delayed received signal used for beamforming in the direction θ |
| $\Phi(t; \theta)$ | Beamformed signal corresponding to the direction θ |
| T | Time duration of the received signal |
| $T_B(\theta)$ | Time duration of the beamformed signal |
| $c_m[k]$ | k th Fourier coefficient of the received signal $\varphi_m(t)$ |
| $\hat{c}[k]$ | k th Fourier coefficient of the beamformed signal $\Phi(t; \theta)$ |
| $\hat{c}_m[k]$ | Auxiliary variable used in deriving frequency-domain beamforming |
| f_s | Beamforming rate |
| $N = \lfloor T \cdot f_s \rfloor$ | Number of samples required by the beamforming rate |
| $q_{k,m}(t; \theta)$ | Distortion function |
| $Q_{k,m;\theta}[n]$ | Fourier coefficients of the distortion function |
| N_1, N_2 | Parameters used for approximation of $c[k]$ |
| β | Effective band-pass bandwidth of the received signal |
| B | Number of Fourier coefficients within β |
| β_{BF} | Effective band-pass bandwidth of the beamformed signal |
| B_{BF} | Number of Fourier coefficients within β_{BF} |
| μ_{BF} | Subset of β_{BF} used for sub-Nyquist processing |
| M_{BF} | Cardinality of μ_{BF} |
| μ | Subset of β required for sub-Nyquist beamforming |
| M | Cardinality of μ |

of the signal. CS recovery from partial frequency data, implying sampling and processing at sub-Nyquist rates, is discussed in Section V. Comparison between the performance of the proposed method with the results obtained in [5] together with an implementation of beamforming in frequency and sub-Nyquist processing on a stand-alone ultrasound machine are presented in Section VI.

Table I summarizes the important notation used throughout the paper.

II. CONVENTIONAL PROCESSING IN ULTRASOUND IMAGING

Most modern imaging systems use multiple transducer elements to transmit and receive acoustic pulses. This allows beamforming during both transmission and reception. Beamforming is a common signal-processing technique [20] that enables spatial selectivity of signal transmission or reception and is applied in various fields, including wireless communication, speech processing, radar, and sonar. In ultrasound imaging, beamforming is used for steering the beam in a desired direction and focusing it in the region of interest to detect tissue structures.

During transmission, beamforming is achieved by delaying the transmission time of each transducer element, which allows the transducer to transmit energy along a narrow beam. Beamforming upon reception is much more challenging. Here, dynamically changing delays are applied on the signals received at each of the transducer elements before averaging. Time-varying delays allow dynamic shift of the reception beam's focal point, optimizing angular resolution. Averaging of the delayed signals in turn enhances the SNR of the resulting beamformed signal, which is used to form a line in an image. From here on, the term beamforming will refer to beamforming upon reception, which is the focus of this work.

A. Beamforming in Time

We begin with a detailed description of the beamforming process which takes place in a typical B-mode imaging cycle. Our presentation is based mainly on [21] and [5]. We will then show, in Section III, how the same process can be performed in frequency, paving the way to substantial rate reduction.

In the transmit path, a pulse is generated and transmitted by the array of transducer elements. The pulse transmitted by each element is timed and scaled, so that the superposition of all transmitted pulses creates a directional beam propagating at a certain angle. By subsequently transmitting at different angles, a whole sector is radiated. The real-time computational complexity in the transmit path is negligible because transmit parameters per angle are calculated offline and saved in tables.

Consider an array comprised of M transceiver elements aligned along the x -axis, as illustrated in Fig. 1. The reference element m_0 is set at the origin and the distance to the m th element is denoted by δ_m . The image cycle begins at $t = 0$, when the array transmits an energy pulse in the direction θ . The pulse propagates through the tissue at speed c , and at time $t \geq 0$ its coordinates are $(x, z) = (ct \sin \theta, ct \cos \theta)$. A potential point reflector located at this position scatters the energy such that the echo is received by all array elements at a time depending on their locations. Denote by $\varphi_m(t)$ the signal received by the m th element and by $\hat{\tau}_m(t; \theta)$ the time of arrival. It is readily seen that

$$\hat{\tau}_m(t; \theta) = t + \frac{d_m(t; \theta)}{c}, \quad (1)$$

where $d_m(t; \theta) = \sqrt{(ct \cos \theta)^2 + (\delta_m - ct \sin \theta)^2}$ is the distance traveled by the reflection. Beamforming involves averaging the signals received by multiple receivers while

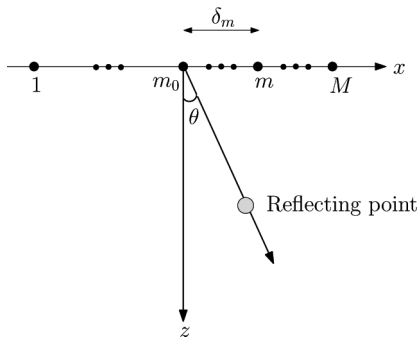


Fig. 1. M receivers aligned along the x -axis. An acoustic pulse is transmitted in a direction θ . The echoes scattered from perturbation in the radiated tissue are received by the array elements.

compensating for the differences in arrival time. In that way, we obtain a signal containing the energy reflected from each point along the central transmission axis θ .

Using (1), the arrival time at m_0 is $\hat{\tau}_{m_0}(t; \theta) = 2t$ because $\delta_{m_0} = 0$. Applying an appropriate delay to $\varphi_m(t)$, such that the resulting signal $\hat{\varphi}_m(t; \theta)$ satisfies $\hat{\varphi}_m(2t; \theta) = \varphi_m(\hat{\tau}_m(t; \theta))$, we can align the reflection received by the m th receiver with the one received at m_0 . Denoting $\tau_m(t; \theta) = \hat{\tau}_m(t/2; \theta)$ and using (1), the following aligned signal is obtained:

$$\begin{aligned} \hat{\varphi}_m(t; \theta) &= \varphi_m(\tau_m(t; \theta)), \\ \tau_m(t; \theta) &= \frac{1}{2} \left(t + \sqrt{t^2 - 4(\delta_m/c)t \sin \theta + 4(\delta_m/c)^2} \right). \end{aligned} \quad (2)$$

The beamformed signal may now be derived by averaging the aligned signals:

$$\Phi(t; \theta) = \frac{1}{M} \sum_{m=1}^M \hat{\varphi}_m(t; \theta). \quad (3)$$

Such a beam is optimally focused at each depth, and hence exhibits improved angular localization and enhanced SNR.

Although defined over continuous time, ultrasound imaging systems perform the beamforming process in (2) and (3) in the digital domain: analog signals $\varphi_m(t)$ are amplified and sampled by an ADC, preceded by an anti-aliasing filter. We next discuss the sampling and processing rates required to perform (3).

B. Rate Requirements

Digital implementation of beamforming requires sampling the signals received at the transducer elements and transmitting the samples to a processing unit. The Nyquist rate, required to avoid aliasing, is insufficient for digital implementation of beamforming because of the high delay resolution needed. Indeed, to apply the delay defined in (2) digitally, received signals must be sampled on a sufficiently dense grid. Typically, the sampling interval is on the order of nanoseconds. Therefore, required sampling rates are significantly higher than the Nyquist rate of the signal and can be as high as hundreds of megahertz [22].

Because of the impracticality of this requirement, ultrasound data are sampled at lower rates, typically on the order of tens of megahertz. Fine delay resolution is obtained by subsequent digital interpolation. Interpolation beamforming allows reduction of the sampling rate at the cost of additional computational load required to implement the digital interpolation, which effectively increases the rate in the digital domain. The processing, or more precisely, beamforming rate, remains unchanged because it is performed at the high digital rate.

Another common way to improve delay accuracy while reducing both sampling and beamforming rate is phase-rotation-based beamforming (PRBF) [2]. In this approach, coarse delays, defined by the sampling rate, are followed by a vernier control, implemented by a digital phase shift, adjusted for the central frequency. The phase shifter approximation to a time delay is exact only at the central frequency, leading to loss in array gain and rise in the side lobe level. The analysis in [2] shows that these losses are dictated by the ratio between the effective bandwidth of the signal and the sampling rate. Therefore, degradation of beam quality can be avoided, provided that the sampling rate is 4 to 10 times the signals' band-pass bandwidth. When assuming that the transducer central frequency is approximately equal to the band-pass bandwidth, we obtain a well-known rule of thumb, requiring sampling rate of 4 to 10 times the transducer central frequency. Hereafter, following [2], we denote the rate required to avoid artifacts in digital implementation of beamforming as the beamforming rate, f_s .

As imaging systems evolve, the number of elements participating in the imaging cycle continues to grow significantly. Consequently large amounts of data must be transmitted from the system front-end and digitally processed in real time. Increasing transmission and processing pose an engineering challenge on digital signal processing (DSP) hardware and motivate reducing the amounts of data as close as possible to the system front-end. This is particularly true for 3-D imaging systems with 2-D transducers. The number of elements in such a transducer is typically above a thousand. Acquiring, and especially transferring, the data from each element is impractical. Instead, only a portion of the entire aperture typically participates in the reception, leading to degradation of the resulting image. Therefore, 3-D imaging can benefit significantly from low-rate sampling.

To conclude this section, we evaluate the sampling rates and the number of samples needed to be taken at each transducer element according to each of the methods described previously. Our evaluation is based on the imaging setup typically used in cardiac imaging. We assume a breadboard ultrasonic scanner of 64 acquisition channels. The radiated depth $r = 16$ cm and speed of sound $c = 1540$ m/s yield a signal of duration $T = 2r/c \simeq 210$ μ s. The acquired signal is characterized by a narrow band-pass bandwidth of 2 MHz, centered at carrier frequency $f_0 \approx 3.4$ MHz. To perform plain delay-and-sum beamforming with 5 ns delay resolution, received signals should be

sampled at the rate of 200 MHz. Implementation of interpolation beamforming, used in many imaging systems, allows reduction of the sampling rate to 50 MHz, while the required beamforming rate is obtained through interpolation in the digital domain. Hence, each channel yields 42000 real-valued samples participating in beamforming. Rates required by PRBF in this setup vary from 8 to 20 MHz, leading to 1680 to 4200 real-valued samples obtained at each transducer element.

It is evident that processing in the time domain imposes a high sampling rate and considerable burden on the beamforming block. We next show that the number of samples can be reduced significantly by exploiting ideas of sub-Nyquist sampling, beamforming in frequency, and CS-based signal reconstruction.

III. BEAMFORMING IN FREQUENCY

We now show that beamforming can be performed equivalently in the frequency domain, paving the way to substantial reduction in the number of samples needed to obtain the same image quality. We extend the notion of compressed beamforming, introduced in [5], to a general concept of beamforming in frequency. In particular, we show that the frequency domain relationship is general and holds irrespective of the FRI model. This allows transfer of the process of beamforming to the frequency domain, while achieving the same result as beamforming in time. We also show that it can be performed efficiently using a small number of Fourier coefficients of the received signals.

A. Implementation and Properties

As mentioned in Section I-B, beamforming in frequency was first addressed in the context of sonar array processing [18], [19], [23]. Sonar, similar to radar, operates in the far field so that the process of beamforming is comprised of steering only. The delays applied to the received signals are defined by the geometry of the array and the steering angle, and are constant in time. Hence, beamforming corresponds to averaging of signals with constant delays. This process can be transferred to the frequency domain in a straightforward manner through the well-known time-shifting property of the Fourier transform: a constant time shift is equivalent to an exponential phase shift in frequency.

In the context of ultrasound imaging, however, dynamic focusing is a crucial step. It allows the focal point to move throughout the scan depth and obtain optimal focusing both in the near field and in the far field. Its implementation, defined in (2), is a nonlinear operation because of time-dependent delays $\tau_m(t; \theta)$ applied to the received signals. Therefore, the fact that the Fourier coefficients of the beam can be obtained as a linear combination of the Fourier coefficients of the received signals does not stem

from the linearity property of the Fourier transform and requires appropriate justification.

We follow the steps in [5] and start from the computation of the Fourier series coefficients of the beam $\Phi(t; \theta)$. As shown in [5], the support of the beam $\Phi(t; \theta)$ is limited to $[0, T_B(\theta))$, where $T_B(\theta) < T$ and T is defined by the transmitted pulse penetration depth. The value of $T_B(\theta)$ is given by [5]

$$T_B(\theta) = \min_{1 \leq m \leq M} \tau_m^{-1}(T; \theta), \quad (4)$$

where $\tau_m(t; \theta)$ is defined in (2). Denote the Fourier series coefficients of $\Phi(t; \theta)$ with respect to the interval $[0, T)$ by

$$c[k] = \frac{1}{T} \int_0^T I_{[0, T_B(\theta))}(t) \Phi(t; \theta) e^{-i(2\pi/T)kt} dt, \quad (5)$$

where $I_{[a, b)}$ is the indicator function equal to 1 when $a \leq t < b$ and 0 otherwise. Plugging (2) and (3) into (5), we get

$$c[k] = \frac{1}{M} \sum_{m=1}^M \hat{c}_m[k], \quad (6)$$

where $\hat{c}_m[k]$ is defined as

$$\hat{c}_m[k] = \frac{1}{T} \int_0^T I_{[0, T_B(\theta))}(t) \varphi_m(\tau_m(t; \theta)) e^{-i(2\pi/T)kt} dt. \quad (7)$$

Our goal is to derive a relationship between the Fourier coefficients of the beam and those of the received signals. To this end, we substitute $x = \tau_m(t; \theta)$. After some algebraic manipulation and replacing x by t , we obtain

$$\hat{c}_m[k] = \frac{1}{T} \int_0^T \varphi_m(t) q_{k,m}(t; \theta) e^{-i(2\pi/T)kt} dt, \quad (8)$$

with

$$q_{k,m}(t; \theta) = I_{[\gamma_m, \tau_m(T; \theta))}(t) \left(1 + \frac{\gamma_m^2 \cos^2 \theta}{(t - \gamma_m \sin \theta)^2} \right) \times \exp \left\{ i \frac{2\pi}{T} k \frac{\gamma_m - t \sin \theta}{t - \gamma_m \sin \theta} \gamma_m \right\}, \quad (9)$$

and $\gamma_m = \delta_m/c$. Note that (8) contains a non-delayed version of $\varphi_m(t)$, in contrast to (7). The delays are effectively applied through the distortion function, $q_{k,m}(t; \theta)$, defined in (9).

We next replace $\varphi_m(t)$ by its Fourier series coefficients. Denoting the n th Fourier coefficient by $c_m[n]$ we can rewrite (8) as

$$\begin{aligned} \hat{c}_m[k] &= \sum_n c_m[n] \frac{1}{T} \int_0^T q_{k,m}(t; \theta) e^{-i(2\pi/T)(k-n)t} dt \\ &= \sum_n c_m[k-n] Q_{k,m;\theta}[n], \end{aligned} \quad (10)$$

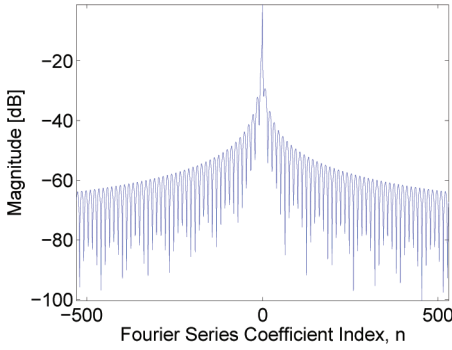


Fig. 2. Fourier coefficients $\{Q_{k,m;\theta}[n]\}$ of $q_{k,m}(t;\theta)$ are characterized by a rapid decay, where most of the energy is concentrated around the DC component. Here, $k = 100$, $m = 14$, and $\theta = 0.421$ rad. 

where $Q_{k,m;\theta}[n]$ are the Fourier coefficients of the distortion function with respect to $[0, T)$. When substituted by its Fourier coefficients, the distortion function effectively transfers the beamforming delays defined in (2) to the frequency domain. The function $q_{k,m}(t;\theta)$ depends only on the array geometry and is independent of the received signals. Therefore, its Fourier coefficients can be computed off-line and used as a look-up-table (LUT) during the imaging cycle. According to proposition 1 in [5], $\hat{c}_m[k]$ can be approximated sufficiently well when we replace the infinite summation in (10) by a finite sum:

$$\hat{c}_m[k] \simeq \sum_{n \in \nu(k)} c_m[k-n] Q_{k,m;\theta}[n]. \quad (11)$$

The set $\nu(k)$ depends on the decay properties of $\{Q_{k,m;\theta}[n]\}$.

We now take a closer look at the properties of $\{Q_{k,m;\theta}[n]\}$. Our numerical studies show that most of the energy of the set $\{Q_{k,m;\theta}[n]\}$ is concentrated around the dc component. This behavior is typical to any choice of k , m , or θ , and is illustrated in Fig. 2 for $k = 100$, $m = 14$, and $\theta = 0.421$ rad. We therefore rewrite (11) as

$$\hat{c}_m[k] \simeq \sum_{n=-N_1}^{N_2} c_m[k-n] Q_{k,m;\theta}[n], \quad (12)$$

where the choice of N_1 and N_2 controls the approximation quality. We assume that for $n < -N_1$ and $n > N_2$, $\{Q_{k,m;\theta}[n]\}$ are several orders of magnitude lower and therefore can be neglected.

In our experiments, we used a 64-element scanner with 0.29 mm element pitch and 120 scanning angles uniformly spanning a 75° sector. For this imaging setup, we found numerically that the 20 most significant elements of $\{Q_{k,m;\theta}[n]\}$ contain, on average, more than 95% of the entire energy irrespective of the choice of k , m , or θ . Beamforming in frequency therefore is performed using the 20 most significant elements in $\{Q_{k,m;\theta}[n]\}$ throughout our work. Such a numerical study can be performed for any phased-array geometry before imaging to estimate the number of elements of $\{Q_{k,m;\theta}[n]\}$ containing the desired percentage of the entire energy.

Substitution of (12) into (6) yields a relationship between the Fourier coefficients of the beam and the individual signals:

$$d[k] \simeq \frac{1}{M} \sum_{m=1}^M \sum_{n=-N_1}^{N_2} c_m[k-n] Q_{k,m;\theta}[n]. \quad (13)$$

Applying an inverse Fourier transform on $\{c[k]\}$ results in the beamformed signal in time. We then proceed to standard image generation steps which include log-compression and interpolation.

To avoid confusion, we emphasize that the distortion function, defined in (9), is not related to the array point spread function (PSF), commonly used in array processing. The array PSF can be viewed as a spatial impulse response of an imaging system, whereas the distortion function we define is a way to treat the nonlinear time-dependent delays that are applied to the received signals in the process of beamforming.

B. Simulations and Validation

To demonstrate the equivalence of beamforming in time and frequency, we applied both methods on *in vivo* cardiac data, yielding the images shown in Fig. 3. The imaging setup is described in Section II-B with $f_s = 16$ MHz for both beamforming in time and in frequency. No rate reduction was applied at this stage. As can be readily seen, the images look identical. Quantitative validation of the proposed method was performed with respect to both one-dimensional beamformed signals and the resulting two-dimensional image.

To compare the one-dimensional signals, we calculated the normalized root-mean-square error (NRMSE) between the signals obtained by beamforming in frequency and those obtained by standard beamforming in time. Both classes of signals were compared after envelope detection, performed by a Hilbert transform to remove the carrier. Denote by $\Phi[n;\theta_j]$ the signal obtained by standard beamforming in direction θ_j , $j = 1, \dots, J$, and let $\hat{\Phi}[n;\theta_j]$ denote the signal obtained by beamforming in frequency. The Hilbert transform is denoted by $H(\cdot)$. For the set of $J = 120$ image lines, we define NRMSE as

$$\text{NRMSE} = \frac{1}{J} \sqrt{\frac{\sum_{n=1}^N (\text{H}(\Phi[n;\theta_j]) - \text{H}(\hat{\Phi}[n;\theta_j]))^2}{\text{H}(\Phi[n;\theta_j])_{\max} - \text{H}(\Phi[n;\theta_j])_{\min}}}, \quad (14)$$

where $\text{H}(\Phi[n;\theta_j])_{\max}$ and $\text{H}(\Phi[n;\theta_j])_{\min}$ denote the maximal and minimal values of the envelope of the beamformed signal in time.

Comparison of the resulting images was performed by calculating the structural similarity (SSIM) index [24], commonly used for measuring similarity between two images. The first line of Table II summarizes the resulting values. These values verify that both one-dimensional signals and the resulting images are extremely similar.

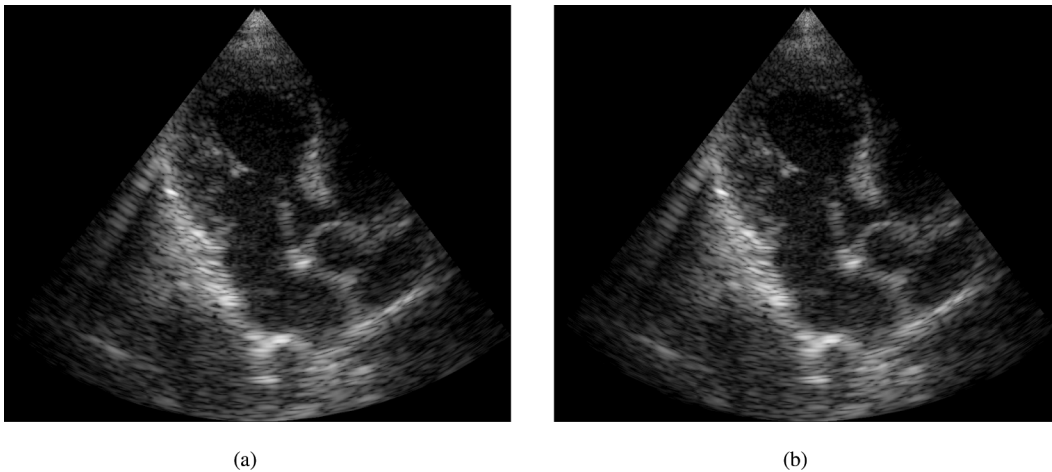


Fig. 3. Cardiac images constructed with different beamforming techniques: (a) time-domain beamforming, (b) frequency-domain beamforming.

IV. RATE REDUCTION BY BEAMFORMING IN FREQUENCY

We next demonstrate that beamforming in frequency allows reduction of the required number of samples of the individual signals. Reduction can be achieved in two different ways. First, we exploit the low effective bandwidth of ultrasound signals and bypass oversampling, dictated by digital implementation of beamforming in time. This allows processing to be performed at the effective Nyquist rate, defined with respect to the effective bandwidth of the signal, which is impossible when beamforming is performed in time. At this stage, the structure of the beamformed signal is not exploited. As a second step, we show that further rate reduction is possible when we take into account the FRI structure of the beamformed signal and use CS techniques for recovery.

We begin this section by addressing rate reduction obtained by frequency-domain beamforming. At this stage, the structure of the beamformed signal is not taken into account.

A. Exploiting the Frequency-Domain Relationship

Denote by β the set of Fourier coefficients of the received signal that correspond to its bandwidth, namely, the values of k for which $c_m[k]$ is nonzero (or larger than a threshold). Let B denote the cardinality of β . Note that (13) implies that the bandwidth of the beamformed signal, β_{BF} , will contain at most $(B + N_1 + N_2)$ nonzero frequency components. In a typical imaging setup, the size of B is on the order of hundreds, whereas N_1 and N_2 , de-

finied by the decay properties of $\{Q_{k,m;\theta}[n]\}$, are typically no larger than 10. This implies that $B + N_1 + N_2 \approx B$, so the bandwidth of the beam is approximately equal to the bandwidth of the received signals.

To compute the elements in β_{BF} according to (13), we need a set β of each of the received signals. This allows exploitation of the low effective bandwidth of the received signals and application of beamforming at a rate corresponding to the effective Nyquist rate of the received signals; namely, the signal's effective band-pass bandwidth. The ratio between the cardinality of the set β and the overall number of samples $N = \lfloor T \cdot f_s \rfloor$, required by the standard beamforming rate f_s , is dictated by the oversampling factor. As mentioned in Section II-B, we define f_s as 4 to 10 times the band-pass bandwidth of the received signal, leading to $B/N = 1/4$ to $1/10$. Assume that it is possible to obtain the required set β for each of the received signals by sampling at the effective Nyquist rate. In this case, the ratio between N and B implies a potential 4- to 10-fold reduction in the required sampling rate.

Having obtained the set β of each one of the received signals, we calculate the elements of β_{BF} by low-rate frequency-domain beamforming. Finally, we reconstruct the beamformed signal in time by performing an inverse Fourier transform. Note that it is possible to pad the elements of β_{BF} with an appropriate number of zeroes to improve time resolution. In our experiments, to compare the proposed method with standard processing, we padded β_{BF} with $N - B$ zeros, leading to the same sampling grid used for high-rate beamforming in time. For the imaging setup described in Section II-B with $f_s = 16$ MHz, we get $N = 3360$ and $B = 416$, leading to an 8-fold rate reduction. We emphasize that this rate reduction is obtained solely by translation of the beamforming operator into the frequency domain without exploiting any structure of the beamformed signal.

Images obtained by the proposed method, using 416 samples per image line to perform beamforming in frequency, and by standard beamforming, using 3360 samples to perform beamforming in time, are shown in Fig. 4.

TABLE II. QUANTITATIVE VALIDATION OF BEAMFORMING IN FREQUENCY WITH RESPECT TO BEAMFORMING IN TIME.

| Method | NRMSE | SSIM |
|---|--------|--------|
| Beamforming in frequency | 0.0349 | 0.9684 |
| Beamforming in frequency, reduced rate sampling | 0.0368 | 0.9603 |

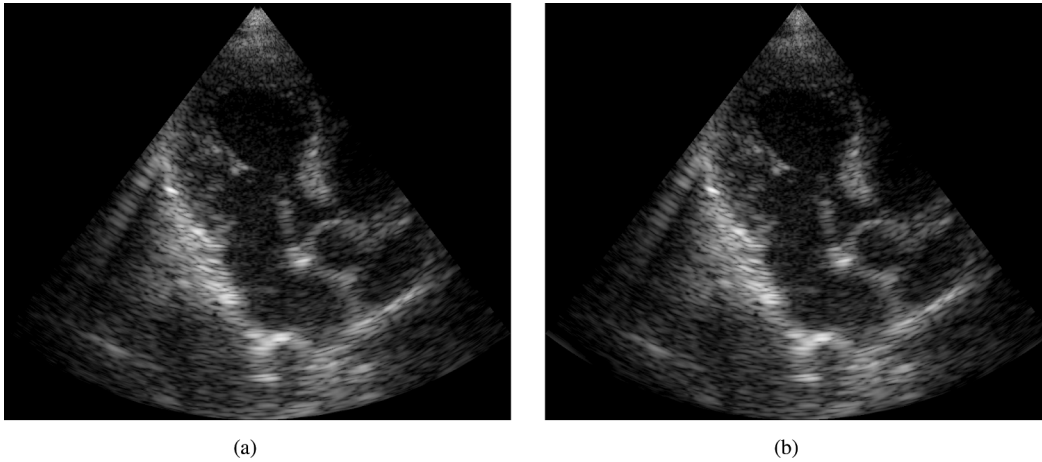


Fig. 4. Cardiac images constructed with different beamforming techniques. (a) Time-domain beamforming. (b) Frequency-domain beamforming, obtained with 8-fold reduction in sampling rate.

Corresponding values of NRMSE and SSIM are reported in the second line of Table II. These values validate close similarity between the two methods. However, in this case, NRMSE is slightly higher and SSIM is lower, compared with the values obtained in Section III-B. Note that these values depict similarity between the signals. Differences can therefore be explained by the following practical aspect. When we obtain the set of all nonzero Fourier coefficients of the beamformed signal, β_{BF} , all the signal energy is captured in the frequency domain. However, the signal obtained by beamforming in time contains noise, which occupies the entire spectrum. When only the Fourier coefficients within the bandwidth are computed in the frequency domain, the noise outside the bandwidth is effectively filtered out. In the signal obtained by standard beamforming, the noise is retained, reducing the similarity between the two signals.

B. Reduced Rate Sampling

To perform beamforming in frequency, we need a certain number of Fourier coefficients of the received signals which is lower than the number of samples required by standard beamforming. However, sampling is performed in time, whereas our goal is to extract the coefficients in the frequency domain. We now address the following question: how do we obtain the required set β corresponding to the effective band-pass bandwidth, using B low-rate samples of each one of the received signals?

A general approach to this problem is to use the Xampling mechanism proposed in [3]. Xampling allows one to obtain an arbitrary set κ , comprised of K frequency components, from K point-wise samples of the signal filtered with an appropriate analog kernel $s^*(-t)$. The kernel is designed according to the required set κ . It effectively zeroes those frequency components of the signal that are not included in κ . The required Fourier coefficients are equal to the Fourier transform of the output; therefore, the number of taken samples is equal to the number of Fourier coefficients of interest. Theoretically, for a general and

possibly nonconsecutive set of frequency components, the sum of sines kernel can be used [3]. Practical aspects of the Xampling approach implementation for sub-Nyquist sampling of radar signals are considered in [11]. This work led to the implementation of a hardware Xampling prototype (see Fig. 5) allowing sampling of radar signals far below their Nyquist rate.

In the context of ultrasound imaging, where a modulated transmitted pulse has one main band of energy, a simpler sampling approach is often possible. We aim to obtain a consecutive set β of the Fourier coefficients of the received signals. This can be achieved by filtering the received signal with a simple band-pass filter corresponding to the frequency band defined by β . The resulting signal can then be sampled at the Nyquist rate, defined with respect to the bandwidth of β , using band-pass [25] or quadrature sampling [26] techniques. Applying the Fourier transform to the resulting low-rate samples yields the required set β . In this approach, the received signals are sampled at their effective Nyquist rate, implying a rate reduction of N/B .

Further reduction in rate can be achieved if we want to obtain only a partial frequency beam's data. Explicitly, assume that now we are interested in $\mu_{\text{BF}} \subset \beta_{\text{BF}}$ of size M_{BF} of Fourier coefficients of the beam. The challenge now is to recover the beam from such partial frequency data, because a simple inverse Fourier transform is insufficient in this case. The recovery, performed by CS, will be discussed in detail in Section V. We note that according

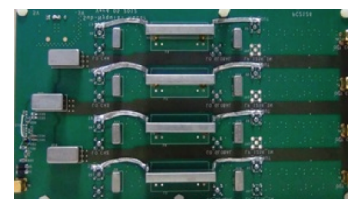


Fig. 5. A Xampling-based hardware prototype for sub-Nyquist sampling. The prototype computes low-rate samples of the input from which the required set of Fourier coefficients can be computed on the outputs. 

to (13), μ_{BF} can be calculated from at most $M = (M_{\text{BF}} + N_1 + N_2)$ Fourier coefficients of each of the received signals. Denote the required subset of M coefficients of the received signal by μ . In this case, the received signals are sampled at a rate which is N/M lower than the standard beamforming rate and B/M lower than their effective Nyquist rate, while the required analog kernel is defined by the subset μ .

The choice of μ , and consequently the analog kernel, is dictated by the transmitted pulse shape. When imaging is performed with a modulated Gaussian pulse, the optimal choice of μ is to take M consecutive elements around the central frequency. This choice captures the maximal amount of the signal energy and can be implemented with a band-pass filter defined by the frequency band corresponding to μ .

On the other hand, if the spectrum of the transmitted pulse is flat, which is the case for linear frequency-modulated chirps [27], [28], then the performance of CS recovery improves when μ is comprised of elements of β chosen uniformly at random. The resulting sampling operation can be implemented using the techniques proposed in [3] and [11].

The entire scheme, performing low-rate sampling and frequency-domain beamforming, is depicted in Fig. 6. Signals $\{\varphi_m(t)\}_{m=1}^M$, received at each transducer element are filtered with an appropriate analog kernel $s^*(-t)$ and sampled at a low rate. Both the analog kernel and the sampling rate are defined by the set of Fourier coefficients of interest. Fourier coefficients of the received signals are then computed and beamforming is performed directly in frequency at a low rate.

V. FURTHER REDUCTION THROUGH COMPRESSED SENSING

We now address reconstruction of the beamformed signal from partial frequency data. Explicitly, we aim to reconstruct the beamformed signal from its M_{BF} Fourier coefficients, denoted by μ_{BF} . To this end, we use CS techniques while exploiting the FRI structure of the beamformed signal. To formulate the recovery as a CS problem, we begin with a parametric representation of the beam. To simplify the notation, we will eliminate the subindex BF in μ_{BF} and M_{BF} throughout this section.

A. Parametric Representation

According to [5], a beamformed signal obeys an FRI model; that is, it can be modeled as a sum of replicas of the known transmitted pulse, $h(t)$, with unknown amplitudes and delays:

$$\Phi(t; \theta) \simeq \sum_{l=1}^L \tilde{b}_l h(t - t_l). \quad (15)$$

Here L is the number of scattering elements in direction θ , $\{\tilde{b}_l\}_{l=1}^L$ are the unknown amplitudes of the reflections, and $\{t_l\}_{l=1}^L$ denote the times at which the reflection from the l th element arrived at the reference receiver m_0 . Because the transmitted pulse is known, such a signal is completely defined by $2L$ unknown parameters: the amplitudes and the delays. The Fourier coefficients of the beam are given by

$$c[k] = h[k] \sum_{l=1}^L \tilde{b}_l e^{-i(2\pi/T)kt_l}, \quad (16)$$

where $h[k]$ is the Fourier coefficient of the transmitted pulse. By quantizing the delays $\{t_l\}_{l=1}^L$ with quantization step $T_s = 1/f_s$, such that $t_l = q_l T_s \in \mathbb{Z}$, we may write the Fourier coefficients of the beamformed signal as

$$c[k] = h[k] \sum_{l=0}^{N-1} b_l e^{-i(2\pi/N)kl}, \quad (17)$$

where $N = \lfloor T/T_s \rfloor$ and

$$b_l = \begin{cases} \tilde{b}_l, & \text{if } l = q_l \\ 0, & \text{otherwise.} \end{cases} \quad (18)$$

We conclude that recovery of the beamformed signal in time is equivalent to determining b_l , $0 \leq l \leq N-1$ in (17).

We now recast the problem in vector-matrix notation. Defining a length- M measurement vector \mathbf{c} with k th entry $c[k]$, $k \in \mu$, we can rewrite (17) as

$$\mathbf{c} = \mathbf{H}\mathbf{D}\mathbf{b} = \mathbf{A}\mathbf{b}, \quad (19)$$

where \mathbf{H} is an $M \times M$ diagonal matrix with $h[k]$ as its k th entry, \mathbf{D} is an $M \times N$ matrix formed by taking the set μ of rows from an $N \times N$ Fourier matrix, and \mathbf{b} is a length- N vector with l th entry b_l . Our goal is to determine \mathbf{b} from \mathbf{c} . We next discuss and compare possible recovery approaches.

B. Prior Work

One approach to determine \mathbf{b} is to view (19) as a complex sinusoid problem. For $M \geq 2L$, it can be solved using

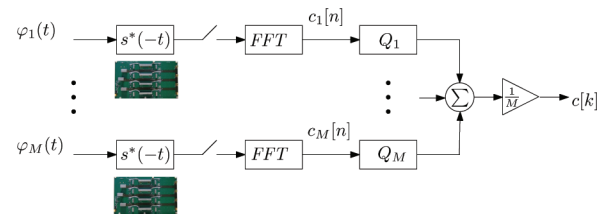


Fig. 6. Fourier-domain beamforming scheme. The block Q_i represents averaging the Fourier coefficients of the received signals with weights $\{Q_{k,m;\theta}[n]\}$ according to (13).

standard spectral analysis methods such as matrix pencil [29] or annihilating filter [30]. Rate reduction is achieved when $2L \ll N$, where N is the number of samples dictated by the standard beamforming rate. In the presence of moderate to high noise levels, the unknown parameters can be extracted more efficiently using a CS approach, as was shown in [5]. Note that (19) is an underdetermined system of linear equations which has infinitely many solutions, because \mathbf{A} is an $M \times N$ matrix with $M \ll N$. The solution set can be narrowed down to a single value by exploiting the structure of the unknown vector \mathbf{b} . In the CS framework, it is assumed that the vector of interest is reasonably sparse, whether in the standard coordinate basis or with respect to some other basis.

The regularization introduced in [5] relies on the assumption that the coefficient vector \mathbf{b} is L -sparse. The formulation in (19) then has a form of a classic CS problem, where the goal is to reconstruct an N -dimensional L -sparse vector \mathbf{b} from its projection onto K orthogonal rows captured by the measurement matrix \mathbf{A} . This problem can be solved using numerous CS techniques when \mathbf{A} satisfies well-known properties such as restricted isometry (RIP) or coherence [6].

In our case, \mathbf{A} , defined in (19), is formed by taking K scaled rows from an $N \times N$ Fourier matrix. It can be shown that by choosing $K \geq CL(\log N)^4$ rows uniformly at random for some positive constant C , the measurement matrix \mathbf{A} obeys the RIP with high probability [31]. In order for this approach to be beneficial, it is important that $L \ll N$. Because random frequency sampling is not practical from a hardware perspective, it is possible instead to sample several frequency bands, distributed randomly throughout the spectrum [11]. This approach is implemented in the board of Fig. 5.

A typical beamformed ultrasound signal is comprised of a relatively small number of strong reflections, corresponding to strong perturbations in the tissue, and many weaker scattered echoes, originating from microscopic changes in acoustic impedance of the tissue. The framework proposed in [5] attempts to recover only strong reflectors in the tissue and treat weak echoes as noise. Hence, the vector of interest \mathbf{b} is indeed L -sparse with $L \ll N$. To recover \mathbf{b} , Wagner *et al.* consider the following optimization problem:

$$\min_{\mathbf{b}} \|\mathbf{b}\|_0 \quad \text{subject to} \quad \|\mathbf{A}\mathbf{b} - \mathbf{c}\|_2 \leq \varepsilon, \quad (20)$$

where ε is an appropriate noise level, and approximate its solution using orthogonal matching pursuit (OMP) [32].

A significant drawback of this method is its inability to restore weak reflectors. In the context of this approach, they are treated as noise and are disregarded by the signal model. As a result, the speckle—the granular pattern that can be seen in Fig. 3—is lost. This severely degrades the value of the resulting images because information carried by speckle is of major importance in many medical imaging modalities. For example, in cardiac imaging, speckle tracking tools allow analysis of the motion of heart tis-

sues and effective tracking of myocardial deformations [33], [34].

C. Alternative Approach

Fortunately, with a small conceptual change of the model, we can restore the entire signal; that is, recover both strong reflectors and weak scattered echoes.

As mentioned previously, a beamformed ultrasound signal is comprised of a relatively small number of strong reflections and many scattered echoes that are, on average, two orders of magnitude weaker. It is therefore natural to assume that the coefficient vector \mathbf{b} , defined in (19), is compressible or approximately sparse, but not exactly sparse. This property of \mathbf{b} can be captured by using the l_1 norm, leading to the optimization problem

$$\min_{\mathbf{b}} \|\mathbf{b}\|_1 \quad \text{subject to} \quad \|\mathbf{A}\mathbf{b} - \mathbf{c}\|_2 \leq \varepsilon. \quad (21)$$

Problem (21) can be solved using second-order methods such as interior point methods [35], [36] or first-order methods, based on iterative shrinkage ideas [37], [38].

We emphasize that although it is common to view (21) as a convex relaxation of (20), in our case, such a substitution is crucial. It allows us to capture the structure of the signal and to boost the performance of sub-Nyquist processing, as will be shown next, through several examples.

The problem of signal reconstruction from partial frequency data can be handled alternatively by an analysis-based approach [39]. In this approach, the set β_{BF} is reconstructed using appropriate l_1 -norm regularization based on signal structure, leading to comparable results [40].

VI. SIMULATIONS AND RESULTS

In this section, we examine the performance of low-rate frequency-domain beamforming using l_1 optimization and compare it to the previously proposed l_0 -based approach. This is done by applying both methods to stored RF data acquired from a healthy volunteer. We then integrate our method into a stand-alone ultrasound machine and show that such processing is feasible in practice using real hardware.

A. Simulations on In Vivo Cardiac Data

To demonstrate low-rate beamforming in frequency and evaluate the impact of rate reduction on image quality, we simulated digitally the application of our technique to *in vivo* cardiac data. The data acquisition setup is described in Section II-B with $f_s = 16$ MHz, leading to $N = 3360$ samples. To perform beamforming in frequency, we used a subset μ_{BF} of 100 Fourier coefficients, which can be obtained from $M = 120$ low-rate samples by the scheme illustrated in Fig. 6 with an appropriate choice of band-pass filter. This implies 28-fold reduction in sam-

pling and 14-fold reduction in processing rate compared with standard beamforming, which requires 3360 samples for this particular imaging setup. The difference between the sampling and processing rates stems from the complex nature of Fourier coefficients. Having computed the Fourier coefficients of the beamformed signal, we obtain its parametric representation by solving (21). To this end, we used the NESTA algorithm [41]. This fast and accurate first-order method, based on the work of Nesterov [42], is shown to be highly suitable for solving (21) when the signal of interest is compressible with high dynamic range, which is particularly true for ultrasound imaging. An additional advantage of NESTA is that it does not depend on fine tuning of numerous controlling parameters. A single smoothing parameter must be selected based on a trade-off between the accuracy of the algorithm and its speed of convergence. This parameter was chosen empirically to yield optimal performance with respect to image quality. To reconstruct the signal, we assumed a noiseless scenario; that is, the parameter ε in (21) was chosen to be zero.

The resulting images, corresponding to two different frames, are shown in Figs. 7(c) and 7(d). Although the images are not identical to those obtained by standard beamforming [Figs. 7(a) and 7(b)], it can be easily seen that l_1 optimization, based on the assumption that the signal of interest is compressible, allows one to reconstruct both strong reflectors and weak echoes. To compare the proposed method with the previously developed l_0 -based approach, we solved (20) with OMP, while assuming $L = 25$ strong reflectors in each direction θ . The resulting images, shown in Figs. 7(e) and 7(f), depict the strong reflectors, observed in Figs. 7(a) and 7(b), while the speckle is lost, degrading the overall image.

To verify the assumption that the weak echoes seen in Figs. 7(c) and 7(d) correspond to fully developed speckle patterns, we evaluated their spatial statistics. According to [43], [44], the amplitude of fully developed speckle obeys a Rayleigh probability density function (pdf). To determine the image regions that follow a Rayleigh pdf, we divided the data, corresponding to the envelope of the image, to overlapping patches of 20×15 pixels. For each patch, the Kolmogorov–Smirnov test (K-S) was applied. This test is a widely used statistical hypothesis test that verifies whether there is enough evidence in data to deduce that the hypothesis under consideration is true. In our case, the hypothesis is that the investigated patch obeys a Rayleigh pdf. The patches that passed the K-S test with significance level $\alpha = 0.05$ were included into the speckle region. This process was performed for images obtained by both standard and low-rate frequency-domain beamforming.

Figs. 8(c) and 8(d) show the speckle regions of images corresponding to frames 1 and 2 obtained by the standard method. The patches that did not pass the test are zeroed out. As can be seen from comparison with the original images, Figs. 8(a) and 8(b), the regions defined by the K-S

test as speckle are in good agreement with our expectation: the strong reflectors such as the valves and the heart wall are excluded while the regions with typical granular structure are preserved. Speckle regions in the images obtained by low-rate frequency-domain beamforming with l_1 -based reconstruction can be seen in Figs. 8(e) and 8(f). As can be seen, there is significant correspondence between the speckle areas. To quantify this correspondence, we defined the speckle area in an image obtained by the standard method as a reference and calculated which percentage of it is defined as speckle in an image obtained by the proposed technique. For frames 1 and 2, the correspondences are 72.99% and 74.10%, respectively.

For completeness, we applied the K-S test to the images obtained by low-rate frequency-domain beamforming with l_0 -based reconstruction, although by construction, this method is not able to recover weak reflectors. As expected, the correspondence in this case is extremely low, 8.48% and 7.68% in frames 1 and 2, respectively.

To conclude, images obtained with 28-fold rate reduction clearly preserve the strong reflectors. In addition, initial spatial statistics analysis allows one to deduce that more than 70% of speckle is retained. A more detailed study of speckle statistics should be performed in future work.

Table III reports corresponding values of NRMSE and SSIM. Although the quantitative values, corresponding to the proposed method with l_1 -based reconstruction, are reduced compared with those obtained in Section IV-B, important information, e.g., the thickness of the heart wall and the valves, as well as the speckle pattern, essential for tracking tools, are preserved. We emphasize that the values of NRMSE and SSIM are provided to give a sense of performance of the proposed method compared with the established technique of time-domain beamforming. In practice, validation is typically performed visually by sonographers, radiologists, and physicians. Furthermore, our approach inherently reduces noise, so high similarity with beamforming in time may not necessarily be advantageous.

B. Implementation on Stand-Alone Imaging System

As a next step, we implemented low-rate frequency-domain beamforming on an ultrasound imaging system [45]. The lab setup used for implementation and testing is shown in Fig. 9 and includes a state-of-the-art GE ultrasound machine, a phantom, and an ultrasound scanning probe. In our study, we used a breadboard ultrasonic scanner with 64 acquisition channels. The radiated depth $r = 15.7$ cm and speed of sound $c = 1540$ m/s yield a signal of duration $T = 2r/c \simeq 204$ μ s. The acquired signal is characterized by a narrow band-pass bandwidth of 1.77 MHz, centered at a carrier frequency $f_0 \approx 3.4$ MHz. The signals are sampled at the rate of 50 MHz and then are digitally demodulated and downsampled to the demodulated processing rate of $f_p \approx 2.94$ MHz, resulting in 1224 samples

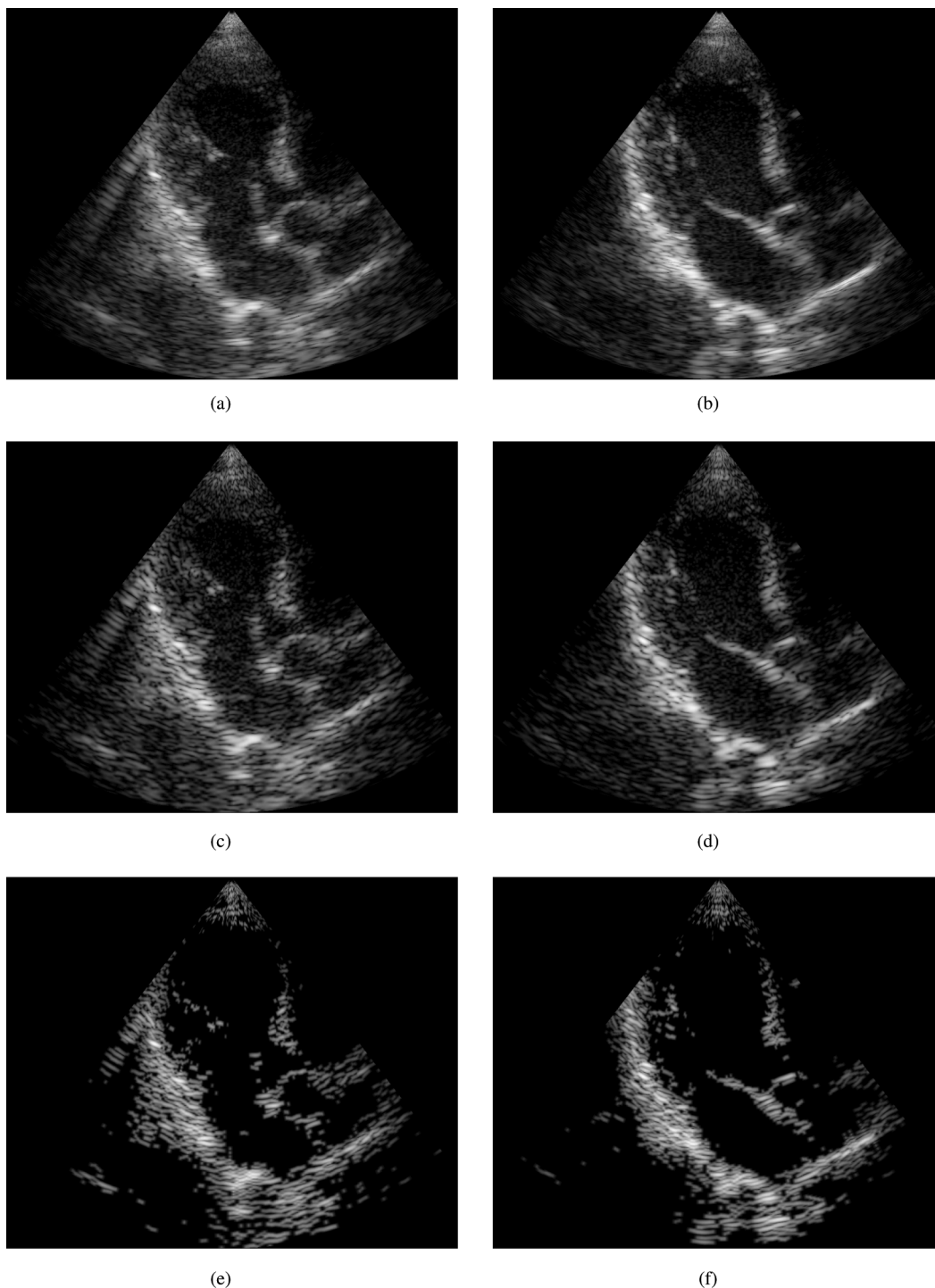


Fig. 7. Experimental results. The first column, (a), (c), (e), corresponds to frame 1; the second column, (b), (d), (f), corresponds to frame 2. (a), (b) Time-domain beamforming. (c), (d) Frequency-domain beamforming, l_1 optimization solution. (e), (f) Frequency-domain beamforming, l_0 optimization solution.

per transducer element. Linear interpolation is then applied to improve beamforming resolution, leading to 2448 samples being used to perform beamforming in time.

Fig. 10 presents a schematic block diagram of the transmit and receive front-end of the medical ultrasound system being used. At this point of our work, as illustrated in Fig. 11, in-phase and quadrature components of the received signals were used to obtain the desired set of

their Fourier coefficients. Using this set, beamforming in frequency was performed according to (13), yielding the Fourier coefficients of the beamformed signal. In this setup, the sampling rate remained unchanged, but frequency-domain beamforming was performed at a low rate. In our experiments, we computed $M_{BF} = 100$ Fourier coefficients of the beamformed signal, using $M = 120$ Fourier coefficients of each of the received signals. This corresponds to

TABLE III. QUANTITATIVE VALIDATION OF BEAMFORMING IN FREQUENCY AT SUB-NYQUIST RATES.

| Method | Frame 1 | | Frame 2 | |
|-----------------------------|---------|--------|---------|--------|
| | NRMSE | SSIM | NRMSE | SSIM |
| l_1 -based reconstruction | 0.0682 | 0.7043 | 0.0587 | 0.6843 |
| l_0 -based reconstruction | 0.0803 | 0.5525 | 0.0697 | 0.5539 |

240 real-valued samples used for beamforming in frequency. The number of samples required by the demodulated processing rate is 2448. Hence, beamforming in frequency is performed at a rate corresponding to $240/2448 \approx 1/10$ of the demodulated processing rate. Images obtained by low-rate beamforming in frequency and standard time-domain beamforming are presented in Fig. 12. As can be

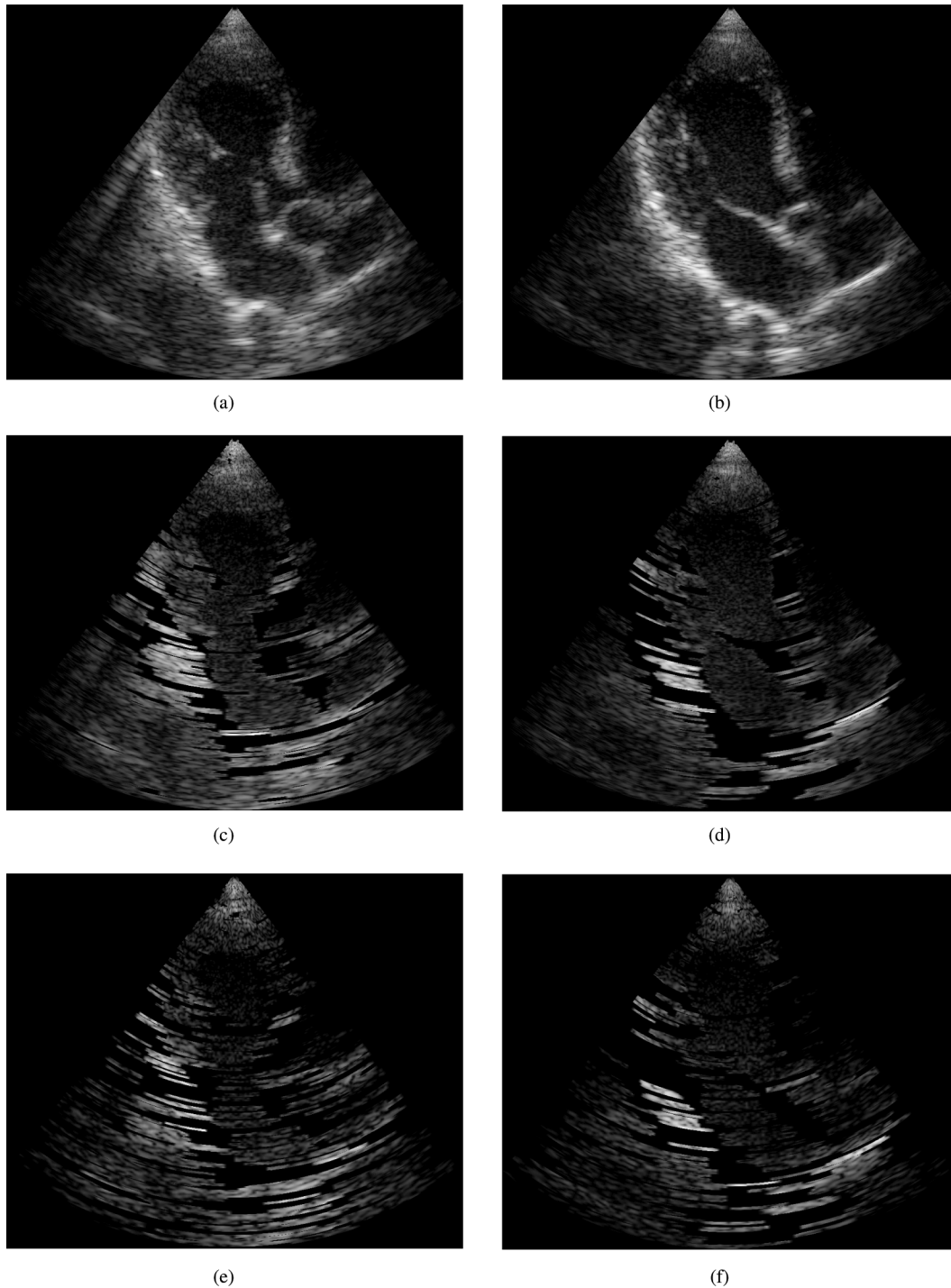


Fig. 8. Speckle pattern preservation. The first column, (a), (c), (e), corresponds to frame 1, the second column, (b), (d), (f), corresponds to frame 2. (a), (b) Time-domain beamforming, original images. (c), (d) Speckle regions, defined by the K-S test within the original images. (e), (f) Speckle regions, defined by the K-S test within the images obtained by low-rate frequency-domain beamforming.



Fig. 9. Lab setup: ultrasound system, probe and cardiac phantom.

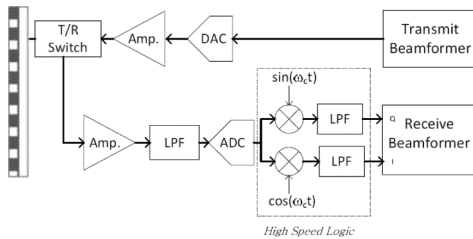


Fig. 10. Transmit and receive front-end of a medical ultrasound system.

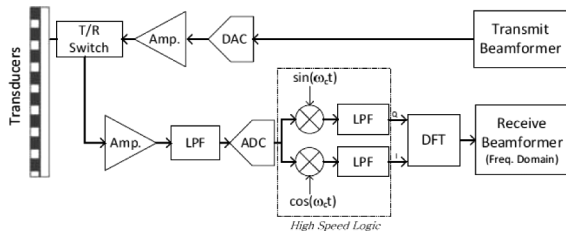


Fig. 11. Transmit and receive paths of a medical ultrasound system with beamforming in the frequency domain.

readily seen, we are able to retain sufficient image quality despite the significant reduction in processing rate.

Our implementation was done on a state-of-the-art system, sampling each channel at a high rate. Data and processing rate reduction took place following the Fourier transform, in the frequency domain. However, by implementing the Xampling scheme described in Section IV-B, the set of 120 Fourier coefficients of the received signals required for frequency-domain beamforming can be obtained directly from only 120 low-rate samples.

VII. DISCUSSION AND CONCLUSIONS

In this work, we propose an entire framework enabling compressed ultrasound imaging, including the step of sub-Nyquist data acquisition, low-rate processing, and beamformed signal reconstruction. The proposed framework is based on Xampling, frequency-domain beamforming, and CS. It allows not only sampling of the received signals at a low rate, but also enables low-rate processing, closing the gap between the acquisition of the raw data and reconstruction of the beamformed signals comprising the resulting image.

We extended the compressed beamforming framework, proposed in [5], to a general concept of beamforming in frequency, equivalent to standard time-domain beamforming. We have shown that when performed directly in frequency, beamforming does not require oversampling, which is essential for its digital implementation in time. Hence, 4- to 10-fold reduction in sampling rate is achieved by the translation of beamforming into the frequency domain, without compromising image quality and without involving any additional assumptions on the signal.

Further reduction in sampling rate is obtained when only a portion of the beam's bandwidth is used. In this case, the received signals are sampled at a sub-Nyquist rate, leading to up to 28-fold reduction in sampling rate. We emphasize that in our approach no projection onto a

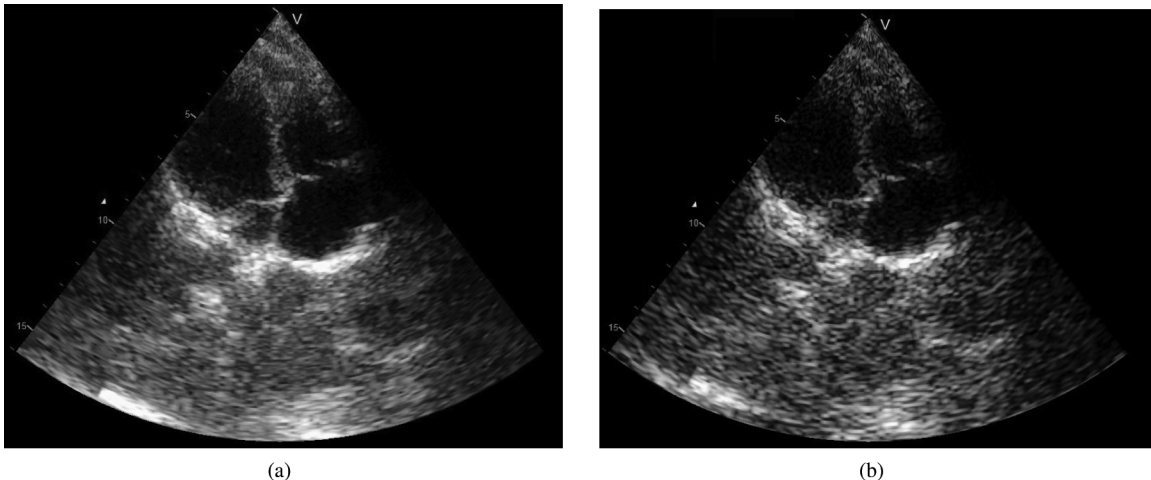


Fig. 12. Cardiac images obtained by demo system. (a) Time-domain beamforming. (b) Frequency-domain beamforming, obtained with 10-fold reduction in processing rate.

random basis before sampling is required. Our Xampling scheme is simple and can be implemented with a band-pass filter.

To reconstruct the beamformed signal from such partial frequency data, we rely on the fact that the beamformed signal obeys an FRI model and use CS techniques. To improve the performance of sub-Nyquist processing and avoid the loss of speckle information, we assumed that the coefficient vector is compressible. This assumption allows one to capture both strong reflections, corresponding to large perturbations in the tissue, and much weaker scattered echoes, originating from microscopic changes in acoustic impedance of the tissue. The latter is initially tested by applying spatial statistical analysis, while a more detailed study of the recovered speckle patterns is left for future work.

Finally, we implemented our frequency-domain beamforming on a stand-alone ultrasound machine. Low-rate processing is performed on the data obtained in real-time by scanning a heart with a 64-element probe. The proposed approach allows for 10-fold rate reduction with respect to the lowest processing rates that are achievable today.

The FRI model implies an assumption that the transmitted pulse shape remains unchanged during its propagation through the tissue. This is, of course, a simplified model of ultrasound propagation, because frequency-dependent attenuation [46, ch. 5] is not taken into account. The results reported in this work can be potentially improved with an appropriate generalization of the FRI model.

Our results prove that the concept of sub-Nyquist processing is feasible for medical ultrasound, leading to the potential of considerable reduction in future ultrasound machines size, power consumption and cost.

ACKNOWLEDGMENTS

The authors thank GE Healthcare Haifa, and in particular Dr. A. Kempinski, for providing the imaging system and for many helpful discussions. They are also grateful to A. Eilam for his assistance with the implementation of the proposed method on an ultrasound machine.

REFERENCES

- [1] C. E. Shannon, "Communication in the presence of noise," *Proc. IRE*, vol. 37, no. 1, pp. 10–21, 1949.
- [2] B. D. Steinberg, "Digital beamforming in ultrasound," *IEEE Trans. Ultrason. Ferroelectr. Freq. Control*, vol. 39, no. 6, pp. 716–721, 1992.
- [3] R. Tur, Y. C. Eldar, and Z. Friedman, "Innovation rate sampling of pulse streams with application to ultrasound imaging," *IEEE Trans. Signal Process.*, vol. 59, no. 4, pp. 1827–1842, 2011.
- [4] M. Vetterli, P. Marziliano, and T. Blu, "Sampling signals with finite rate of innovation," *IEEE Trans. Signal Process.*, vol. 50, no. 6, pp. 1417–1428, 2002.
- [5] N. Wagner, Y. C. Eldar, and Z. Friedman, "Compressed beamforming in ultrasound imaging," *IEEE Trans. Signal Process.*, vol. 60, no. 9, pp. 4643–4657, 2012.
- [6] Y. C. Eldar and G. Kutyniok, *Compressed Sensing: Theory and Applications*. Cambridge, UK: Cambridge University Press, 2012.
- [7] K. Gedalyahu, R. Tur, and Y. C. Eldar, "Multichannel sampling of pulse streams at the rate of innovation," *IEEE Trans. Signal Process.*, vol. 59, no. 4, pp. 1491–1504, 2011.
- [8] T. Michaeli and Y. C. Eldar, "Xampling at the rate of innovation," *IEEE Trans. Signal Process.*, vol. 60, no. 3, pp. 1121–1133, 2011.
- [9] M. Mishali, Y. C. Eldar, O. Dounaevsky, and E. Shoshan, "Xampling: Analog to digital at sub-Nyquist rates," *IET Circuits Devices Syst.*, vol. 5, no. 1, pp. 8–20, 2011.
- [10] M. Mishali, Y. C. Eldar, and A. J. Elron, "Xampling: Signal acquisition and processing in union of subspaces," *IEEE Trans. Signal Process.*, vol. 59, no. 10, pp. 4719–4734, 2011.
- [11] E. Baransky, G. Itzhak, I. Shmuel, N. Wagner, E. Shoshan, and Y. C. Eldar, "A sub-Nyquist radar prototype: Hardware and algorithms," *IEEE Trans. Aerosp. Electron. Syst.*, 2012, submitted for publication.
- [12] X. Zhuang, Y. Zhao, Z. Dai, H. Wang, and L. Wang, "Ultrasonic signal compressive detection with sub-nyquist sampling rate," *J. Sci. Ind. Res.*, vol. 71, pp. 195–199, Mar. 2012.
- [13] J. Zhou, Y. He, M. Chirala, B. M. Sadler, and S. Hoyos, "Compressed digital beamformer with asynchronous sampling for ultrasound imaging," in *IEEE Int. Conf. Acoustics, Speech and Signal Processing*, 2013, pp. 1056–1060.
- [14] H. Liebgott, R. Prost, and D. Friboulet, "Pre-beamformed rf signal reconstruction in medical ultrasound using compressive sensing," *Ultrasonics*, vol. 53, no. 2, pp. 525–533, 2012.
- [15] A. Achim, B. Buxton, G. Tzagarakis, and P. Tsakalides, "Compressive sensing for ultrasound rf echoes using a-stable distributions," in *Annu. Int. Conf. IEEE Engineering in Medicine and Biology Society*, 2010, pp. 4304–4307.
- [16] G. Tzagarakis, A. Achim, P. Tsakalides, and J.-L. Starck, "Joint reconstruction of compressively sensed ultrasound rf echoes by exploiting temporal correlations," in *IEEE 10th Int. Symp. Biomedical Imaging*, 2013, pp. 632–635.
- [17] C. Quinsac, A. Basarab, and D. Kouamé, "Frequency domain compressive sampling for ultrasound imaging," *Adv. Acoust. Vib.*, vol. 2012, art. no. 231317, 2012.
- [18] J. R. Williams, "Fast beam-forming algorithm," *J. Acoust. Soc. Am.*, vol. 44, no. 5, pp. 1454–1455, 1968.
- [19] P. Rudnick, "Digital beamforming in the frequency domain," *J. Acoust. Soc. Am.*, vol. 46, no. 5A, pp. 1089–1090, 1969.
- [20] H. L. Van Trees, *Detection, Estimation, and Modulation Theory, Optimum Array Processing*. New York, NY: Wiley-Interscience, 2004.
- [21] J. A. Jensen, "Linear description of ultrasound imaging systems," in *Notes for the International Summer School on Advanced Ultrasound Imaging, Technical University of Denmark July*, 5, 1999.
- [22] M. O'Donnell, W. E. Engeler, J. T. Pedicone, A. M. Itani, S. E. Noujaim, R. J. Dunki-Jacobs, W. M. Leue, C. L. Chalek, L. S. Smith, J. E. Piel, R. L. Harris, K. B. Welles, and W. L. Hinrichs, "Real-time phased array imaging using digital beam forming and autonomous channel control," in *Proc. IEEE Ultrasonics Symp.*, 1990, pp. 1499–1502.
- [23] G. DeMuth, "Frequency domain beamforming techniques," in *IEEE Int. Conf. Acoustics, Speech, and Signal Processing*, 1977, vol. 2, pp. 713–715.
- [24] Z. Wang, A. C. Bovik, H. R. Sheikh, and E. P. Simoncelli, "Image quality assessment: From error visibility to structural similarity," *IEEE Trans. Image Process.*, vol. 13, no. 4, pp. 600–612, 2004.
- [25] R. G. Vaughan, N. L. Scott, and D. R. White, "The theory of band-pass sampling," *IEEE Trans. Signal Process.*, vol. 39, no. 9, pp. 1973–1984, 1991.
- [26] O. D. Grace and S. P. Pitt, "Sampling and interpolation of bandlimited signals by quadrature methods," *J. Acoust. Soc. Am.*, vol. 48, no. 6A, pp. 1311–1318, 1970.
- [27] T. Misaridis and J. A. Jensen, "Use of modulated excitation signals in medical ultrasound. Part I: Basic concepts and expected benefits," *IEEE Trans. Ultrason. Ferroelectr. Freq. Control*, vol. 52, no. 2, pp. 177–191, 2005.
- [28] J. M. G. Borsboom, C. T. Chin, A. Bouakaz, M. Versluis, and N. de Jong, "Harmonic chirp imaging method for ultrasound contrast agent," *IEEE Trans. Ultrason. Ferroelectr. Freq. Control*, vol. 52, no. 2, pp. 241–249, 2005.
- [29] T. K. Sarkar and O. Pereira, "Using the matrix pencil method to estimate the parameters of a sum of complex exponentials," *IEEE Antennas Propagat. Mag.*, vol. 37, no. 1, pp. 48–55, 1995.

- [30] P. Stoica and R. L. Moses, *Introduction to Spectral Analysis*, vol. 89, Upper Saddle River, NJ: Prentice Hall, 1997.
- [31] M. Rudelson and R. Vershynin “On sparse reconstruction from fourier and gaussian measurements,” *Commun. Pure Appl. Math.*, vol. 61, no. 8, pp. 1025–1045, 2008.
- [32] J. A. Tropp and A. C. Gilbert, “Signal recovery from random measurements via orthogonal matching pursuit,” *IEEE Trans. Inf. Theory*, vol. 53, no. 12, pp. 4655–4666, 2007.
- [33] Y. Notomi, P. Lysyansky, R. M. Setser, T. Shiota, Z. B. Popovic, M. G. Martin-Miklovic, J. A. Weaver, S. J. Oryszak, N. L. Greenberg, R. D. White, and J. D. Thomas, “Measurement of ventricular torsion by two-dimensional ultrasound speckle tracking imaging,” *J. Am. Coll. Cardiol.*, vol. 45, no. 12, pp. 2034–2041, 2005.
- [34] M. S. Suffoletto, K. Dohi, M. Cannesson, S. Saba, and J. Gorcsan, “Novel speckle-tracking radial strain from routine black-and-white echocardiographic images to quantify dyssynchrony and predict response to cardiac resynchronization therapy,” *Circulation*, vol. 113, no. 7, pp. 960–968, 2006.
- [35] E. Candès and J. Romberg. (2007). l_1 -magic: Recovery of sparse signals via complex programming. [Online]. Available: <http://users.ece.gatech.edu/justin/l1magic/downloads/l1magic.pdf>
- [36] M. Grant, S. Boyd, and Y. Ye. (2008). CVX: Matlab software for disciplined convex programming. [Online]. Available: <http://www.stanford.edu/~boyd/cvx>
- [37] A. Beck and M. Teboulle “A fast iterative shrinkage-thresholding algorithm for linear inverse problems,” *SIAM J. Imaging Sci.*, vol. 2, no. 1, pp. 183–202, 2009.
- [38] E. T. Hale, W. Yin, and Y. Zhang, “A fixed-point continuation method for l_1 -regularized minimization with applications to compressed sensing,” CAAM Technical Report TR07–07, Rice University, Houston, TX, 2007.
- [39] E. J. Candes, Y. C. Eldar, D. Needell, and P. Randall, “Compressed sensing with coherent and redundant dictionaries,” *Appl. Comput. Harmon. Anal.*, vol. 31, no. 1, pp. 59–73, 2011.
- [40] T. Chernyakova, Y. C. Eldar, and R. Amit, “Fourier domain beamforming for medical ultrasound,” in *Int. Conf. Acoustics, Speech and Signal Processing*, 2013, pp. 924–928.
- [41] S. Becker, J. Bobin, and J. Emmanuel, “Candès. NESTA: A fast and accurate first-order method for sparse recovery,” *SIAM J. Imaging Sci.*, vol. 4, no. 1, pp. 1–39, 2011.
- [42] Y. Nesterov, “Smooth minimization of non-smooth functions,” *Math. Program.*, vol. 103, no. 1, pp. 127–152, 2005.
- [43] C. B. Burckhardt, “Speckle in ultrasound b-mode scans,” *IEEE Trans. Sonics Ultrason.*, vol. 25, no. 1, pp. 1–6, 1978.
- [44] R. F. Wagner, S. W. Smith, J. M. Sandrik, and H. Lopez, “Statistics of speckle in ultrasound b-scans,” *IEEE Trans. Sonics Ultrason.*, vol. 30, no. 3, pp. 156–163, 1983.
- [45] A. Eilam, T. Chernyakova, Y. C. Eldar, and A. Kempinski, “Sub-Nyquist medical ultrasound imaging: En route to cloud processing,” in *IEEE Global Conf. Signal and Information Processing*, 2013, art. no. NSSIMb.PD.3.
- [46] H. Azhari, *Basics of Biomedical Ultrasound for Engineers*. New York, NY: Wiley, 2010.



Yonina C. Eldar (S'98–M'02–SM'07–F'12) received the B.Sc. degree in physics and the B.Sc. degree in electrical engineering, both from Tel-Aviv University (TAU), Tel-Aviv, Israel, in 1995 and 1996, respectively, and the Ph.D. degree in electrical engineering and computer science from the Massachusetts Institute of Technology (MIT), Cambridge, MA in 2002.

From January 2002 to July 2002, she was a Postdoctoral Fellow at the Digital Signal Processing Group at MIT. She is currently a Professor in the Department of Electrical Engineering at the Technion–Israel Institute of Technology, Haifa, and holds the Edwards Chair in Engineering. She is also a Research Affiliate with the Research Laboratory of Electronics at MIT and a Visiting Professor at Stanford University, Stanford, CA. Her research interests are in the broad areas of statistical signal processing, sampling theory and compressed sensing, optimization methods, and their applications to biology and optics.

Dr. Eldar was in the program for outstanding students at TAU from 1992 to 1996. In 1998, she held the Rosenblith Fellowship for study in electrical engineering at MIT, and in 2000, she held an IBM Research Fellowship. From 2002 to 2005, she was a Horev Fellow of the Leaders in Science and Technology program at the Technion and an Alon Fellow. In 2004, she was awarded the Wolf Foundation Krill Prize for Excellence in Scientific Research; in 2005, the Andre and Bella Meyer Lectureship; in 2007, the Henry Taub Prize for Excellence in Research; in 2008, the Hershel Rich Innovation Award, the Award for Women with Distinguished Contributions, the Muriel and David Jacknow Award for Excellence in Teaching, and the Technion Outstanding Lecture Award; in 2009, the Technion's Award for Excellence in Teaching; in 2010, the Michael Bruno Memorial Award from the Rothschild Foundation; and in 2011, the Weizmann Prize for Exact Sciences. In 2012, she was elected to the Young Israel Academy of Science and to the Israel Committee for Higher Education, and elected an IEEE Fellow. In 2013, she received the Technion's Award for Excellence in Teaching, the Hershel Rich Innovation Award, and the IEEE Signal Processing Technical Achievement Award, and in 2014, the IEEE/AESS Fred Nathanson Memorial Radar Award. She received several best paper awards together with her research students and colleagues. She is the Editor-in-Chief of *Foundations and Trends in Signal Processing* and a member of the IEEE Sensor Array and Multichannel Technical Committee. In the past, she was a Signal Processing Society Distinguished Lecturer, a member of the IEEE Signal Processing Theory and Methods and Bio Imaging Signal Processing technical committees, and she served as an associate editor for the *IEEE Transactions on Signal Processing*, the *EURASIP Journal of Signal Processing*, the *SIAM Journal on Matrix Analysis and Applications*, and the *SIAM Journal on Imaging Sciences*.



Tanya Chernyakova received the B.Sc. degree in biomedical engineering (Cum Laude) from the Technion–Israel Institute of Technology, Haifa, in 2011. She is currently pursuing the Ph. D. degree in electrical engineering at the Technion–Israel Institute of Technology. Her research interests include theoretical aspects of signal processing, sampling theory, compressed sensing, medical imaging, and advanced signal processing methods for ultrasonic imaging. In 2013, Ms. Chernyakova was an Ollendorff fellow and in 2014 she was awarded the David and Tova Freud and Ruth Freud-Brendel Memorial Scholarship.